CHEMISTRY
AN ASIAN JOURNAL

www.chemasianj.org

Accepted Article

Title: Superior Electrocatalysis Delivered by a Directional Electron Transfer Cascade in Hierarchical CoNi/Ru@C

Authors: Mingpu Jia, Ling Shen, Ge Tian, Susana I. Córdoba de Torresi, Mark D. Symes, and Xiao-Yu Yang

To be cited as: *Chem. Asian J.* **2022**, e202200449

Link to VoR: https://doi.org/10.1002/asia.202200449

A Journal of

ACES
Asian Chemical Editorial Society

A sister journal of **Angewandte Chemie** and **Chemistry – A European Journal**

WILEY-VCH

RESEARCH ARTICLE WILEY-VCH

Superior Electrocatalysis Delivered by a Directional Electron Transfer Cascade in Hierarchical CoNi/Ru@C

Mingpu Jia,[a] Ling Shen,[a] Ge Tian,*[a] Susana I. Córdoba de Torresi,[b] Mark D. Symes,[c] and Xiao-Yu Yang*[a]

[a] M. Jia, L. Shen, Dr. G. Tian, Prof. Dr. X.-Y. Yang
State Key Laboratory of Advanced Technology for Materials Synthesis and Processing
International School of Materials Science and Engineering
School of Materials Science and Engineering
Shenzhen Research Institute
Joint Laboratory for Marine Advanced Materials in Pilot National Laboratory for Marine Science and Technology (Qingdao)
Wuhan University of Technology
Wuhan, 430070, China
E-mail: xyyang@whut.edu.cn
[b] Prof. Dr. S. I. Córdoba de Torresi
Instituto de Química
Universidade de Sao Paulo
Av. Prof. Lineu Prestes 748, 05508-080 São Paulo, SP, Brazil
[c] Dr. M. D. Symes
WestCHEM School of Chemistry
University of Glasgow
Glasgow, G12 8QQ, UK

Supporting information for this article is given via a link at the end of the document.

Abstract: Exploiting directional electron transfer cascades could lead to high-performance electrocatalysts for processes such as the hydrogen evolution reaction, but realising such systems is difficult. Herein, a hierarchical confined material (CoNi/Ru@C) is presented, which provides a suitable spatial junction to enable directional electron transfer, giving superior hydrogen evolution in alkaline water/seawater.

Introduction

Ruthenium (Ru) has been widely studied in electrocatalysis, such as the hydrogen and oxygen evolution reactions (HER and OER),[1-3] and many successful approaches have been developed to improve the electrocatalytic activity of Ru.[4-9] One such approach involves alloying or doping Ru with more electropositive metals, in order to modulate the electron density on Ru. For example, electron transfer from transition metals such as Ni and Co to Ru can result in outstanding electrocatalytic activities.[10-13] A similar, albeit electronically reversed effect, can be seen in materials where metals such as Ru are mixed with non-metals (e.g. Ru can be mixed with carbon), where the superior performance of these materials can be ascribed to removal of electron density from the metal by the more electronegative non-metals.[14-16] In light of these previous results, it is possible that further improvements in the activity of Ru could be realised by combining the electronic effects of different additional metals and non-metals. There are many successful examples of ternary compositions containing Ru, another transition metal and a non-metal, such as Ru-Co-C and Ru-Ni-C, both of which display high activity for the HER.[17,18] However, directional electron density transfer from these other transition metals to Ru, and then from Ru to carbon is rarely reported, because the Co (or Ni) and Ru atoms in the Ru-Co (Ni) alloys studied to date are uniformly dispersed. Therefore, transfer of electron density between Co (or Ni) and Ru does occur, but only between neighbouring atoms.[10,19] Directional electron transfer over larger length scales (e.g. across the interfaces of domains of Ru and Co (or Ni), rather than merely between individual atoms) is difficult to achieve. Directed transfer of electron density brings to mind natural photosynthesis, where photogenerated electrons transfer in a highly efficient cascade.[20] Our aim, therefore, was to create a spatial junction comprised of a transition metal, Ru and a non-metal, which would enable Ru to gain electron density from the transition metal and then transfer this to the non-metal, resulting in a directional electron transfer cascade, which we hypothesised would in turn lead to enhanced electrocatalysis.

Confined nanostructures are perfect candidates for inducing such electron transfer cascades.[21-27] Consider, for example, an inorganic electron transfer chain where a CoNi alloy acts as the electron donor (with Co and Ni having electronegativities of 1.88 and 1.91, respectively), carbon as the electron acceptor (electronegativity = 2.50) and Ru (electronegativity = 2.20) in the middle. Herein, just such a CoNi/Ru@C spatial junction has been designed and synthesised. The optimal CoNi/Ru@C formulation shows outstanding HER performance, requiring an overpotential of only 14 mV to deliver a current density of 10 mA cm^{-2}, and with good stability for 20 h in alkaline medium (superior to the performance exhibited by commercial Pt/C). Furthermore, in simulated seawater, such a spatial junction also shows a very low overpotential requirement to reach 10 mA cm^{-2} of only 6 mV, again with better stability than that shown by Pt/C.

Results and Discussion

The synthetic route to CoNi/Ru@C is illustrated in Figure 1a. CoNi@C is dispersed in an aqueous $RuCl_3$ solution, and then Ru^{3+} undergoes galvanic replacement with CoNi inside the carbon shell (at 100 °C, hydrothermal conditions),[28,29] which leads to the formation of a CoNi/Ru alloy with a junction

structure confined within a carbon case. The pristine CoNi@C has a lamellar structure consisting of many nanoparticles (Figure S1a, a1). After introducing Ru, the morphology of the sample does not change with increasing Ru content, indicating the maintenance of the initial structure of CoNi@C and possible Ru replacement only in the CoNi core (Figure S1a-f1). HAADF-STEM and TEM images (Figure 1b and f) also show the thin layer structure of CoNi/Ru@C with high dispersion of the alloying nanoparticles, and the energy dispersive X-ray spectroscopy (EDX) mapping images show that the Co, Ni and Ru are uniformly dispersed in the sample (Figure 1c-e). The high-resolution TEM (HRTEM, Figure 1g, i-k) images confirm that there is a spatial junction consisting of CoNi, Ru, and carbon. The lattice fringe with spacings of 0.203 and 0.214 nm correspond to the (111) plane of Co or Ni and (002) plane of Ru (Figure 1i).[30,31] Moreover, the spacings of 0.182 and 0.239 nm correspond to the (220) plane of Co or Ni and the (100) plane of Ru, respectively (Figure 1j).[32] These results indicate the formation of a CoNi/Ru alloy with a junction structure and a spatial junction consisting of CoNi/Ru@carbon as shown in Figure 1k.

The powder X-ray diffraction (XRD, Figure 1h, S2) shows that the peak intensity of CoNi (111) at 44.5° gradually reduces with increasing Ru content in the samples (1.9, 4.0, 5.7, 6.3, 7.0 wt% Ru taken from the ICP-OES results (Table S1), named as CoNi/Ru@C-X wt%, where X represents the Ru content). Note that no new peak occurs in CoNi/Ru@C after introducing Ru in comparison with CoNi@C (the peaks at 25.5° and 44.5° correspond to C (002) and CoNi (111), respectively). This is directly due to the very small size of Ru and CoNi and the influence of a broad peak of carbon at around 44° (Figure S3).

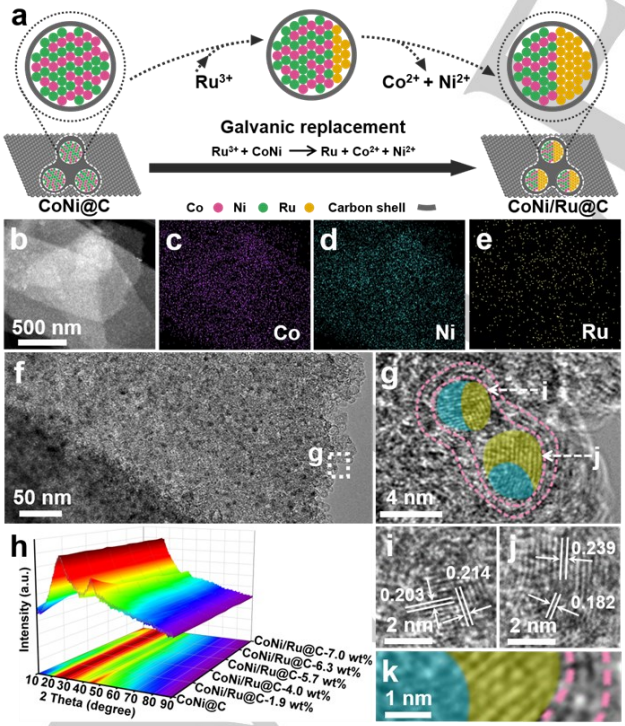

Figure 1. (a) The synthetic route to CoNi/Ru@C. (b) HAADF-STEM image and (c-e) EDX Mapping images of Co, Ni, Ru element distribution. (f) TEM and (g, i-k) HRTEM images of CoNi/Ru@C. (h) XRD patterns of CoNi@C and CoNi/Ru@C.

The electrochemical properties were then evaluated by a three-electrode system in 1 M N_2-saturated KOH solution. It can be seen from the LSV curves that under cathodic bias, the samples exhibited non-zero currents, suggesting HER catalytic activity, and CoNi/Ru@C materials with different Ru contents have different activities (Figure S4). We find that inadequate or excessive Ru contents cause a lower HER efficiency, with the optimal initial content being 6.3 wt% Ru in CoNi/Ru@C (Figure S5, see detail description in Supporting Information). To demonstrate the significant activity improvement of confined structured CoNi/Ru@C, commercial Pt/C (Pt: 20 wt%), commercial Ru/C (Ru: 5 wt%) and CoNiRu/C (as a mixture of Co, Ni, Ru and C by co-reduction on a C support, as a control sample of random junction alloying) were chosen for comparison. The significant activity differences of CoNi/Ru@C, Pt/C, Ru/C, CoNiRu/C and CoNi@C can be seen from their LSV curves (Figure 2a). Specifically, the overpotentials of these samples at different current densities are also compared (Figure 2b). The overpotential of CoNi/Ru@C (14 mV) at a current density of 10 mA cm^{-2} is obviously smaller than that of Pt/C (41 mV), Ru/C (71 mV), CoNiRu/C (132 mV) and CoNi@C (254 mV), respectively. Even at larger current densities (50 and 100 mA cm^{-2}), CoNi/Ru@C still shows the smallest overpotential (48 and 75 mV, respectively) in comparison with the control samples. The mass activity of these samples was also analysed through normalizing the currents to the noble metal mass of the catalysts (Figure S7). The current density of CoNi/Ru@C is 0.42 mA μg^{-1} at the overpotential of 10 mV, which is 9 and 5 times larger than Pt/C (0.04 mA μg^{-1}) and Ru/C (0.07 mA μg^{-1}). And at overpotentials of 50 mV and 100 mV, the current density of CoNi/Ru@C (3.28 and 10.38 mA μg^{-1}) is almost an order of magnitude larger than that of Pt/C (0.28 and 0.93 mA μg^{-1}) and Ru/C (0.39 and 1.67 mA μg^{-1}). These results demonstrate that

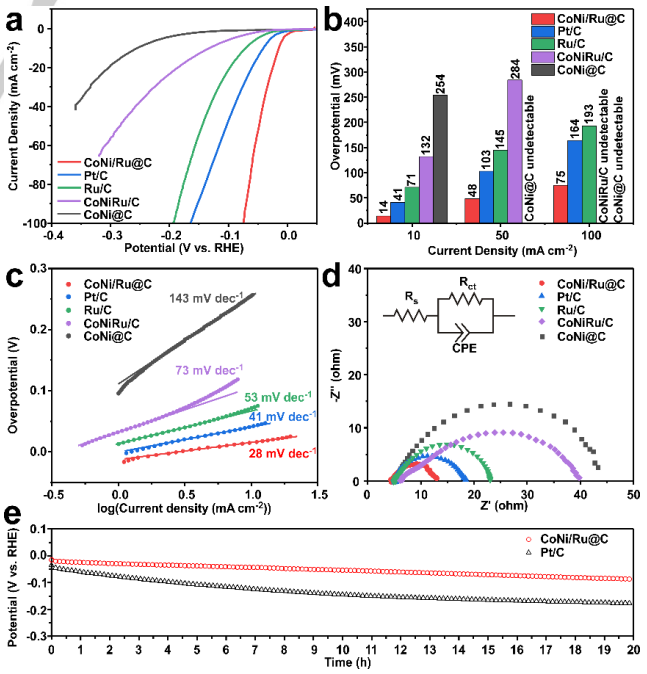

Figure 2. (a) LSV curves with IR correction, (b) Overpotential at current densities of 10, 50, 100 mA cm^{-2}, (c) Tafel plots and (d) EIS plots of CoNi/Ru@C, Pt/C, Ru/C, CoNiRu/C and CoNi@C. (e) Chronopotentiometry curves of Pt/C and CoNi/Ru@C in 1 M KOH solution.

CoNi/Ru@C has the best HER catalytic activity in 1 M KOH, compared with those commercial HER catalysts. Moreover, its activity also outperforms most of the reported alkaline HER electrocatalysts (Table S3). The Tafel slope of CoNi/Ru@C is 28 mV dec^{-1}, which is smaller than that of Pt/C (41 mV dec^{-1}), Ru/C (53 mV dec^{-1}), CoNiRu/C (73 mV dec^{-1}) and CoNi@C (143 mV dec^{-1}) (Figure 2c), demonstrating that the spatial junction of CoNi/Ru@C greatly boosts HER kinetics.[33,34] The charge transfer resistance (R_{ct}) of Pt/C (13.1 Ω), Ru/C (18.6 Ω), CoNiRu/C (37.1 Ω) and CoNi@C (40.9 Ω) are larger than that of CoNi/Ru@C (8.5 Ω), implying CoNi/Ru@C has a higher charge-transfer rate and faster catalytic kinetics (Figure 2d and Table S2).[35,36] This result is in good agreement with the catalytic activity from the LSV curves. Durability is a significant parameter for comparing electrocatalysts.[37] The chronopotentiometry curves of CoNi/Ru@C and commercial Pt/C were measured at a constant current density of 10 mA cm^{-2} (Figure 2e). It is obvious that the required potential for CoNi/Ru@C increases much less than for Pt/C, suggesting superior stability for CoNi/Ru@C.

Electrocatalytic seawater splitting is seen as a promising route for the sustainable production of H_2, because of the vast reservoir of seawater as the input material.[38-40] However, the high salinity and compositional complexity of seawater present challenges in terms of electrocatalyst deactivation and undesirable side reactions.[41] Carbon shell structures display good corrosion resistance towards seawater and enable enhanced photo/electro catalytic performances.[42,43] The electrochemical HER catalytic activities of confined structured CoNi/Ru@C were therefore tested in alkaline simulated seawater (1 M KOH + 3.5 wt% NaCl solution) (Figure 3).[44,45] The overpotential of CoNi/Ru@C at a current density of 10 mA cm^{-2} is only 6 mV, which is much smaller than that of Pt/C (24 mV) (Figure 3b). The Tafel slope of CoNi/Ru@C is calculated to

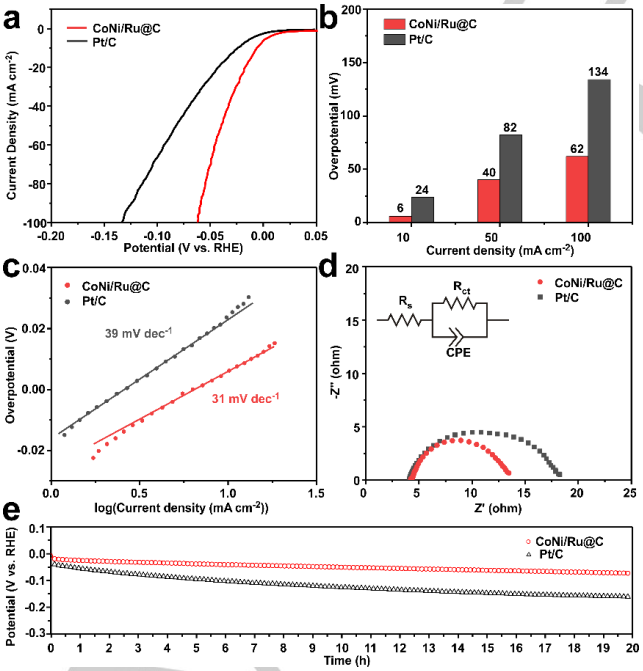

Figure 3. (a) LSV curves with IR correction, (b) Overpotential at current densities of 10, 50 and 100 mA cm^{-2}, (c) Tafel plots, (d) EIS plots and (e) Chronopotentiometry curves of CoNi/Ru@C and Pt/C in 1 M KOH + 3.5 wt% NaCl solution.

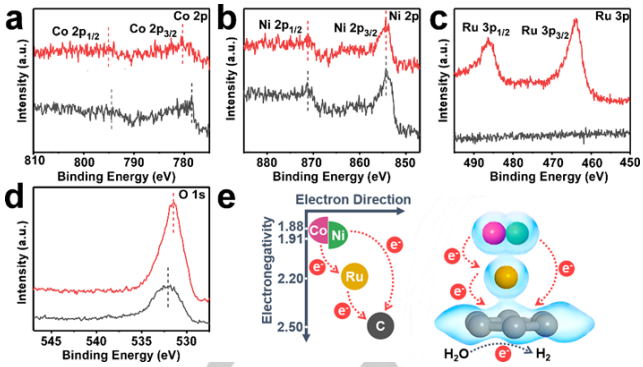

Figure 4. High-resolution XPS spectra (a) Co 2p, (b) Ni 2p, (c) Ru 3p and (d) O 1s of CoNi/Ru@C (red line) and CoNi@C (black line). (e) Schematic illustration of the directional electron transfer cascade in CoNi/Ru@C.

be 31 mV dec^{-1}, which is smaller than that of Pt/C (39 mV dec^{-1}), suggesting favourable reaction kinetics for CoNi/Ru@C (Figure. 3c). Moreover, the smaller R_{ct} of CoNi/Ru@C indicates that it has a better electrode-electrolyte interface dynamic (Figure 3d). Furthermore, after a 20 h chronopotentiometry test, CoNi/Ru@C was found to show superior stability in alkaline simulated seawater (Figure 3e).

The high activity and stability of CoNi/Ru@C could be due to the unique spatial junction structure. The evidence for directed electron transfer caused by this junction is shown in the XPS spectra of CoNi/Ru@C and CoNi@C. It can be confirmed that CoNi/Ru@C is composed of C, N, O, Co, Ni and Ru (Figure S8). The two main peaks at 464.2 eV and 486.4 eV are assigned to Ru $3p_{3/2}$ and Ru $3p_{1/2}$ of metallic Ru in CoNi/Ru@C (Figure 4c).[46] Meanwhile, the Co 2p and Ni 2p peaks of CoNi/Ru@C shift toward higher binding energy compared to CoNi@C (Figure 4a and b), implying that there is electronic coupling between CoNi and Ru and that electrons transfer from CoNi to Ru.[10,19,46-48] As is well-known, it is difficult to directly determine the peak shift of C 1s because C is used to calibrate samples (Figure S9).[49] The O peak from the carbon shell was therefore chosen to determine the extent of electron transfer to the carbon shell. In the high-resolution O 1s spectra (Figure 4d), the peak of O 1s of CoNi/Ru@C is negatively shifted, indicating a higher electron density.[16] It is reasonable to deduce that the electrons of Ru, and also from CoNi, transfer to C.[21,50] The electron transfer chain from CoNi to Ru to C, suggested by XPS, is in accordance with the spatial junction structure CoNi/Ru@C observed by TEM. The spatial junction we propose (Figure 4e) shows the cascade effect of electron transfer, wherein the electron transfers from the Co and/or Ni to the Ru, and then to the carbon shell following the law of electronegativity. This directional effect greatly modulates the electronic structure of the Ru, leading to the highly efficient utilization of electrons during electrocatalysis. The outer carbon shell aids in this, not only by acting as an electron acceptor, but also by protecting the inner alloy metals from the harsh outside environment.[51] Finally, HER occurs on the carbon shell, including the dissociation of water, hydrogen adsorption (H^*) and then the recombination of two H^* intermediates to give gaseous hydrogen.[52] As a comparison, in the presence of just CoNi and Ru, or in the presence of random alloys of CoNiRu on carbon supports, the HER electrocatalytic activity of these structures is comparatively poorer.

Conclusion

In summary, a spatial junction in a hierarchical confined structured CoNi/Ru@C material has been successfully fabricated through a facile galvanic replacement. Due to the directional electron transfer cascade in this structure, the alkaline HER performance of hierarchical CoNi/Ru@C is dramatically promoted (14 mV overpotential and 20 hours' stability), even for the splitting of seawater (6 mV overpotential and 20 hours' stability). It is believed that our work can provide a versatile strategy for producing efficient catalysts for energy technologies.

Experimental Section

Chemicals: Ethylenediaminetetraacetic acid tetrasodium salt hydrate ($Na_4EDTA{\cdot}2H_2O$), nickel nitrate hexahydrate ($Ni(NO_3)_2{\cdot}6H_2O$), nickel chloride hexahydrate ($NiCl_2{\cdot}6H_2O$), ruthenium on carbon (Ru/C), ruthenium chloride hydrate ($RuCl_3{\cdot}xH_2O$) and Nafion117 solution were purchased from Aladdin Biochemical Technology Co., Ltd. Commercial Pt/C (20 wt% Pt) was purchased from Johnson Matthey Corp. Cobalt nitrate hexahydrate ($Co(NO_3)_2{\cdot}6H_2O$), cobalt chloride hexahydrate ($CoCl_2{\cdot}6H_2O$), sulfuric acid (H_2SO_4), potassium hydroxide (KOH), sodium chloride (NaCl), sodium borohydride ($NaBH_4$), methanol and ethanol absolute were purchased from Sinopharm Chemical Reagent Co., Ltd. All chemicals were used without further purification.

Synthesis of CoNi@C: The synthesis of CoNi@C was performed according to a previous work.[21] Typically, 12 mmol $Na_4EDTA{\cdot}2H_2O$, 12 mmol $Co(NO_3)_2{\cdot}6H_2O$ and 12 mmol $Ni(NO_3)_2{\cdot}6H_2O$ were dissolved in 15 mL ultrapure water. After the addition of 10 mL methanol, the obtained purple mixture was then transferred into a 40 mL-autoclave and kept at 200 °C for 24 h. After cooling down, the precipitate was collected through vacuum filtration and washed with ultrapure water and dried at 100 °C. The obtained light purple solid was then ground to fine powder and carbonized at 475 °C for 3 h under the flow of Ar. The as-prepared black powder was treated with 0.5 M H_2SO_4 for 4 h at 90 °C. After cooling down, the precipitate was collected through vacuum filtration and washed with plenty of ultrapure water and finally dried in a vacuum oven to obtain CoNi@C.

Synthesis of CoNi/Ru@C: 30 mg CoNi@C was uniformly dispersed in 10 mL ultrapure water under ultrasonic irradiation, then 5 mL ultrapure water containing 50 μL, 100 μL, 150 μL, 200 μL or 250 μL 0.2 M $RuCl_3$ aqueous solution was added under vigorous stirring, respectively. The mixture was then sealed in a 25 mL-autoclave and kept at 100 °C for 9 h. After cooling down, the precipitate was collected through vacuum filtration and washed with ultrapure water and finally dried at 60 °C in a vacuum oven.

Synthesis of CoNiRu/C: 43.5 mg Ru/C was dispersed in 4 mL ultrapure water under ultrasonic irradiation, and then 60 μL 0.2 M $CoCl_2$ aqueous solution and 83 μL 0.2 M $NiCl_2$ aqueous solution were added. Finally, 1 mL ultrapure water containing 9.4 mg $NaBH_4$ was quickly injected into the above mixture under vigorous stirring. After stirring for another 30 min, the as-synthesized CoNiRu/C was collected through vacuum filtration and washed with ultrapure water and finally dried at 60 °C in a vacuum oven.

Material characterization: The scanning electron microscopy (SEM, Hitachi S-4800) was conducted to study the morphology of materials. The transmission electron microscope (TEM, ThermoFisher Talos F200S) was applied to gain further detailed information about the structure and composition of materials. X-ray diffraction (XRD, Bruker D8-Advance X-ray diffractometer) operating with Cu Kα radiation was carried out to study the phase and composition of materials. Inductively Coupled Plasma-Optical Emission Spectroscopy (ICP-OES, Prodigy 7) was applied to analyze the content of metal elements in the catalysts. X-ray photoelectron spectroscopy (XPS, AXIS SUPRA) was employed to analyze the elemental composition and chemical state of the materials.

Electrochemical measurement: A three-electrode system was used to test the electrocatalysis of the as-obtained samples. In order to prepare the ink, 5 mg catalyst was dispersed in the mixture of 980 μL ethanol and 20 μL Nafion117 under ultrasonic irradiation. 10 μL catalyst ink was dropped on the rotating disk electrode (RDE), served as working electrode. Graphite rod and reversible hydrogen electrode (RHE) were served as counter electrode and reference electrode, respectively. 1 M N_2-saturated KOH solution was used as the electrolyte. The rotating rate of the rotating disk electrode was set as 1600 rpm. Before linear sweep voltammetry (LSV) measurement, cyclic voltammetry (CV) measurement was performed between -0.2 V and 0.05 V (vs. RHE) with the scan rate of 100 mV s^{-1} until a steady CV curve was obtained. The LSV was then carried out with the potential from 0.05 V to -0.3 V (vs. RHE) with the scan rate of 5 mV s^{-1}. The electrochemical double-layer capacitance (C_{dl}) is calculated from the CV curves at scan rates of 20, 40, 60, 80 and 100 mV s^{-1} in a narrow potential range between 0.1 and 0.2 V (vs. RHE). The electrochemical impedance spectroscopy (EIS) was tested at the corresponding potentials of 10 mA cm^{-2} from LSV curves, with the frequency range between 0.1 Hz and 100 KHz.

Note that the above LSV curves were all collected at least twice, and in all cases the repeats were found to be similar.

Acknowledgements

This work was supported by NSFC (51861135313), the National 111 project (B20002), PCSIRT (IRT_15R52), Sino-German Centre's COVID-19 Related Bilateral Collaborative Project (C-0046), Guangdong Province International Scientific and Technological Cooperation Projects (2020A0505100036), Shenzhen Science and Technology Program (JCYJ20210324142010029). Guangdong Basic and Applied Basic Research Foundation (2022A1515010137, 2022A1515010504). MDS thanks the Royal Society for a University Research Fellowship (UF150104). We thank the Nanostructure Research Centre (NRC) for the S/TEM work.

Conflict of Interest

The authors declare no conflict of interest.

Keywords: Ru-based alloying • directional electrocatalysis • cascade electron transfer • hydrogen production from seawater

[1] W. Luo, Y. Wang, C. Cheng, *Mater. Today Phys.* **2020**, *15*, 100274.
[2] X. Cui, P. Ren, C. Ma, J. Zhao, R. Chen, S. Chen, N. P. Rajan, H. Li, L. Yu, Z. Tian, D. Deng, *Adv. Mater.* **2020**, *32*, 1908126.
[3] A. R. Poerwoprajitno, L. Gloag, T. M. Benedetti, S. Cheong, J. Watt, D. L. Huber, J. J. Gooding, R. D. Tilley, *Small* **2019**, *15*, 1804577.
[4] X. Kong, K. Xu, C. Zhang, J. Dai, S. Norooz Oliaee, L. Li, X. Zeng, C. Wu, Z. Peng, *ACS Catal.* **2016**, *6*, 1487–1492.
[5] Z. Pu, I. S. Amiinu, Z. Kou, W. Li, S. Mu, *Angew. Chem. Int. Ed.* **2017**, *56*, 11559–11564.

[6] T. Zhu, J. Huang, B. Huang, N. Zhang, S. Liu, Q. Yao, S. Haw, Y. Chang, C. Pao, J. Chen, Q. Shao, Z. Hu, Y. Ma, X. Huang, *Adv. Energy Mater.* **2020**, *10*, 2002860.

[7] Y. Li, L. A. Zhang, Y. Qin, F. Chu, Y. Kong, Y. Tao, Y. Li, Y. Bu, D. Ding, M. Liu, *ACS Catal.* **2018**, *8*, 5714–5720.

[8] J. Wang, Z. Wei, S. Mao, H. Li, Y. Wang, *Energy Environ. Sci.* **2018**, *11*, 800–806.

[9] H. Li, K. Liu, J. Fu, K. Chen, K. Yang, Y. Lin, B. Yang, Q. Wang, H. Pan, Z. Cai, H. Li, M. Cao, J. Hu, Y.-R. Lu, T.-S. Chan, E. Cortés, A. Fratalocchi, M. Liu, *Nano Energy* **2021**, *82*, 105767.

[10] Y. Liu, X. Li, Q. Zhang, W. Li, Y. Xie, H. Liu, L. Shang, Z. Liu, Z. Chen, L. Gu, Z. Tang, T. Zhang, S. Lu, *Angew. Chem. Int. Ed.* **2020**, *59*, 1718–1726.

[11] W. Li, Y. Zhao, Y. Liu, M. Sun, G. I. N. Waterhouse, B. Huang, K. Zhang, T. Zhang, S. Lu, *Angew. Chem. Int. Ed.* **2021**, *60*, 3290–3298.

[12] Y. Wang, H. Yu, J. Ying, G. Tian, Y. Liu, W. Geng, J. Hu, Y. Lu, G. Chang, K. I. Ozoemena, C. Janiak, X. Yang, *Chem. Eur. J.* **2021**, *27*, 9124–9128.

[13] C. Cai, K. Liu, Y. Zhu, P. Li, Q. Wang, B. Liu, S. Chen, H. Li, L. Zhu, H. Li, J. Fu, Y. Chen, E. Pensa, J. Hu, Y. Lu, T. Chan, E. Cortés, M. Liu, *Angew. Chem. Int. Ed.* **2022**, *61*, DOI 10.1002/anie.202113664.

[14] Y.-X. Xiao, J. Ying, G. Tian, Y. Tao, H. Wei, S.-Y. Fan, Z.-H. Sun, W.-J. Zou, J. Hu, G.-G. Chang, W. Li, X.-Y. Yang, C. Janiak, *Appl. Catal. B-Environ.* **2019**, *259*, 118080.

[15] Y. Wu, X. Li, Y. Wei, Z. Fu, W. Wei, X. Wu, Q. Zhu, Q. Xu, *Adv. Mater.* **2021**, *33*, 2006965.

[16] P. Su, W. Pei, X. Wang, Y. Ma, Q. Jiang, J. Liang, S. Zhou, J. Zhao, J. Liu, G. Q. (Max) Lu, *Angew. Chem. Int. Ed.* **2021**, *60*, 16044–16050.

[17] J. Su, Y. Yang, G. Xia, J. Chen, P. Jiang, Q. Chen, *Nat. Commun.* **2017**, *8*, 14969.

[18] Q. Yang, P. Jin, B. Liu, L. Zhao, J. Cai, Z. Wei, S. Zuo, J. Zhang, L. Feng, *J. Mater. Chem. A* **2020**, *8*, 9049–9057.

[19] B. Sarkar, D. Das, K. K. Nanda, *Green Chem.* **2020**, *22*, 7884–7895.

[20] Y. Lu, X.-L. Liu, L. He, Y.-X. Zhang, Z.-Y. Hu, G. Tian, X. Cheng, S.-M. Wu, Y.-Z. Li, X.-H. Yang, L.-Y. Wang, J.-W. Liu, C. Janiak, G.-G. Chang, W.-H. Li, G. Van Tendeloo, X.-Y. Yang, B.-L. Su, *Nano Lett.* **2020**, *20*, 3122–3129.

[21] J. Deng, P. Ren, D. Deng, X. Bao, *Angew. Chem. Int. Ed.* **2015**, *54*, 2100–2104.

[22] X. Cui, P. Ren, D. Deng, J. Deng, X. Bao, *Energy Environ. Sci.* **2016**, *9*, 123–129.

[23] J. Deng, D. Deng, X. Bao, *Adv. Mater.* **2017**, *29*, 1606967.

[24] Y. Tu, P. Ren, D. Deng, X. Bao, *Nano Energy* **2018**, *52*, 494–500.

[25] Y. Tu, J. Deng, C. Ma, L. Yu, X. Bao, D. Deng, *Nano Energy* **2020**, *72*, 104700.

[26] Y. Wang, P. Ren, J. Hu, Y. Tu, Z. Gong, Y. Cui, Y. Zheng, M. Chen, W. Zhang, C. Ma, L. Yu, F. Yang, Y. Wang, X. Bao, D. Deng, *Nat. Commun.* **2021**, *12*, 5814.

[27] L. Shen, J. Ying, K. I. Ozoemena, C. Janiak, X.-Y. Yang, *Adv. Funct. Mater.* **2021**, 2110851.

[28] Y.-X. Xiao, J. Ying, G. Tian, X.-Q. Zhang, C. Janiak, K. I. Ozoemena, X.-Y. Yang, *Chem. Commun.* **2021**, *57*, 986–989.

[29] Y.-X. Xiao, J. Ying, G. Tian, X. Yang, Y.-X. Zhang, J.-B. Chen, Y. Wang, M. D. Symes, K. I. Ozoemena, J. Wu, X.-Y. Yang, *Nano Lett.* **2021**, *21*, 7870–7878.

[30] W. Wang, S. Xi, Y. Shao, W. Sun, S. Wang, J. Gao, C. Mao, X. Guo, G. Li, *ACS Sustainable Chem. Eng.* **2019**, *7*, 17227–17236.

[31] Y. Zhou, Z. Xie, J. Jiang, J. Wang, X. Song, Q. He, W. Ding, Z. Wei, *Nat. Catal.* **2020**, *3*, 454–462.

[32] Y. Guo, Z. Chen, R. M. Rioux, P. E. Savage, *J. Supercrit. Fluid.* **2019**, *143*, 336–345.

[33] A. P. Murthy, J. Theerthagiri, J. Madhavan, *J. Phys. Chem. C* **2018**, *122*, 23943–23949.

[34] J. Cai, J. Ding, D. Wei, X. Xie, B. Li, S. Lu, J. Zhang, Y. Liu, Q. Cai, S. Zang, *Adv. Energy Mater.* **2021**, *11*, 2100141.

[35] L. Tian, X. Yan, X. Chen, *ACS Catal.* **2016**, *6*, 5441–5448.

[36] C. Cheng, S. S. A. Shah, T. Najam, X. Qi, Z. Wei, *Electrochim. Acta* **2018**, *260*, 358–364.

[37] Z. Chen, H. Qing, K. Zhou, D. Sun, R. Wu, *Prog. Mater. Sci.* **2020**, *108*, 100618.

[38] C. Wang, H. Shang, L. Jin, H. Xu, Y. Du, *Nanoscale* **2021**, *13*, 7897–7912.

[39] Z. Yu, Y. Duan, X. Feng, X. Yu, M. Gao, S. Yu, *Adv. Mater.* **2021**, *33*, 2007100.

[40] G. Liu, Y. Xu, T. Yang, L. Jiang, *Nano Materials Science* **2020**, S2589965120300659.

[41] W. Zheng, L. Y. S. Lee, K.-Y. Wong, *Nanoscale* **2021**, *13*, 15177–15187.

[42] Y. Lu, Y.-X. Liu, L. He, L.-Y. Wang, X.-L. Liu, J.-W. Liu, Y.-Z. Li, G. Tian, H. Zhao, X.-H. Yang, J. Liu, C. Janiak, S. Lenaerts, X.-Y. Yang, B.-L. Su, *Nanoscale* **2020**, *12*, 8364–8370.

[43] T.-C. Yang, F.-C. Chang, H. P. Wang, Y.-L. Wei, C.-J. Jou, *Mar. Pollut. Bull.* **2014**, *85*, 696–699.

[44] N. Jiang, H.-M. Meng, L.-J. Song, H.-Y. Yu, *Int. J. Hydrogen Energ.* **2010**, *35*, 8056–8062.

[45] S. Pareek, D. Jain, D. Behera, S. Sharma, R. Shrivastava, *Materials Today: Proceedings* **2021**, *43*, 3303–3308.

[46] H. Gao, J. Zang, X. Liu, Y. Wang, P. Tian, S. Zhou, S. Song, P. Chen, W. Li, *Appl. Surf. Sci.* **2019**, *494*, 101–110.

[47] L. Wang, Z. Tang, W. Yan, Q. Wang, H. Yang, S. Chen, *J. Power Sources* **2017**, *343*, 458–466.

[48] D. Li, Z. Zong, Z. Tang, Z. Liu, S. Chen, Y. Tian, X. Wang, *ACS Sustainable Chem. Eng.* **2018**, *6*, 5105–5114.

[49] D. Fang, F. He, J. Xie, L. Xue, *J. Wuhan Univ. Technol.-Mat. Sci. Edit.* **2020**, *35*, 711–718.

[50] J. Kim, Y. Yang, A. Seong, H.-J. Noh, C. Kim, S. Joo, A. Cho, L. Zhang, J. Zhou, J.-Q. Wang, J. W. Han, J. Mahmood, J.-B. Baek, G. Kim, *J. Mater. Chem. A* **2020**, *8*, 14927–14934.

[51] L. Yu, D. Deng, X. Bao, *Angew. Chem. Int. Ed.* **2020**, *132*, 15406–15409.

[52] D. Strmcnik, P. P. Lopes, B. Genorio, V. R. Stamenkovic, N. M. Markovic, *Nano Energy* **2016**, *29*, 29–36.

Entry for the Table of Contents

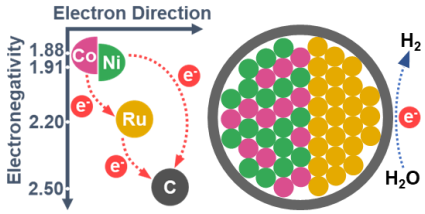

The spatial junction in hierarchical confined CoNi/Ru@C has been synthesized, and its directional effect of electron transfer cascade can greatly promote the electrocatalytic hydrogen evolution in alkaline water/seawater.